ELSEVIER

Available online at www.sciencedirect.com
ScienceDirect
Journal of Hydrodynamics
2008,20(1):74-80

sdlj.chinajournal.net.cn

NUMERICAL SIMULATION OF HORIZONTAL MIGRATION OF PROPPANT*

ZHAO Zheng-chao, CUI Bin, YUE Yu-quan
Institute of Mechanics, Chinese Academy of Sciences, Beijing 100080, China
Liao'he Oilfield, Panjing 124010, China, E-mail: zhaozc@petrochina.com.cn
WANG Li-yang, WU Ying-xiang
Institute of Mechanics, Chinese Academy of Sciences, Beijing 100080, China

(Received April 19, 2007, Revised August 8, 2007)

Abstract: The horizontal migration of proppant was numerically investigated with a two-fluid model, in which the interaction between fracturing fluid and proppant, along with that among proppants was taken into account through interphase forces. The migration process and the volumetric concentration of the proppant were examined under various conditions, and the averaged volumetric concentration of the proppant was obtained. The present research might be useful in the process design of the hydraulic fracturing in the oilfields.

Key words: numerical simulation,two-fluid model, two-phase flow,hoirzontal migration

1. Introduction

Hydraulic fracturing, used to form a high-diversion-capability crack inside proppant, is an effective way of transforming reservoirs and improving the production of oil/gas wells. Therefore, it is necessary to understand and control the proppant migration behavior inside sand-carrying agent. The flowback is undesirable in the oilfield because it would reduce the effective supporting scales, and consequently, lower the diversion capabilities. Furthermore, the flowback may plug the well bores, erode the ground facilities, and increse the security costs. The investigation on the proppant migration inside cracks during hydraulic fracturing is a key subject for researchers engaged in reservoir simulation [1-6].

The theoretical analysis and experiments on hydraulic fracturing using proppant are very difficult due to its inherent complexity of physical and meahcnical processes. Numerical simulation has been, therefore, often used. The convection-diffusion model based on classical diffusion theory was often applied [7, 8], in which a set of partial differential equations for fracturing fluid and convection-diffusion equations were solved.

For hydraulic fracturing with a high volumetric concentration of proppant, the above model is not applicable as the interphasic interaction is neglected, and in this case the two-fluid model [9-11] is considered to be more reasonable and reliable. In the two-fluid model, two sets of partial differential equations describing the sediment and water, along with the coupled equations of interphase forces are solved together. In the present study, therefore, the two-fluid model is used to investigate the proppant migration at the initial stage of mandatory closing operations under different conditions.

2. Mathematical model

2.1 *Volumetric Fraction*

The description of multiphase flow as interpenetrating continua involves the concept of phasic volumetric fraction denoted by α_q, which represents the space occupied by each phase, and the

* Project supported by "Eleventh Five-Year Plan" of the Chinese Academy of Sciences (Grant No. KJCX2-YW-L02).
Biography: ZHAO Zheng-chao (1961-), Male, Ph. D. Student, Professor

laws of conservation of mass and momentum are satisfied by each phase individually. The derivation of the conservation equations can be performed by ensemble averaging the local instantaneous balance for each phase [12], and the physical variables are obtained through time-averaging [13].

The volume V_q for the phase q is defined by

$$V_q = \int_V \alpha_q \mathrm{d}V \tag{1}$$

where

$$\sum_{q=1}^{n} \alpha_q = 1 \tag{2}$$

2.2 *Conservation equations*

2.2.1Conservation of mass

By neglecting the mass transfer between phases, the continuity equation for the phase q is given as

$$\frac{\partial}{\partial t}(\alpha_q \rho_q) + \nabla \cdot (\alpha_q \rho_q \boldsymbol{v}_q) = 0 \tag{3}$$

where, $\boldsymbol{v}_q$ and ρ_q are the velocity and density of the phase q respectively.

2.2.2 Conservation of momentum

The momentum balance for the phase q yields [14]:

$$\frac{\partial}{\partial t}\left(\alpha_q \rho_q \boldsymbol{v}_q\right) + \nabla \cdot \left(\alpha_q \rho_q \boldsymbol{v}_q \boldsymbol{v}_q\right) = -\alpha_q \nabla p + \nabla \cdot \overline{\overline{\boldsymbol{\tau}}}_q + \alpha_q \rho_q \boldsymbol{g} + \alpha_q \rho_q (\boldsymbol{F}_q + \boldsymbol{F}_{lift,q} + \boldsymbol{F}_{Vm,q}) + \sum_{p=1}^{n} K_{pq}(\boldsymbol{v}_p - \boldsymbol{v}_q) \tag{4}$$

where $\overline{\overline{\boldsymbol{\tau}}}_q$ is the q^{th} phase stress-strain tensor [15]:

$$\overline{\overline{\boldsymbol{\tau}}}_q = \alpha_q \mu_q (\nabla \boldsymbol{v}_q + \nabla \boldsymbol{v}_q^{\,T}) + \alpha_q (\lambda_q - \frac{2}{3}\mu_q) \nabla \cdot \boldsymbol{v}_q \overline{\overline{\mathbf{I}}} \tag{5}$$

Herein, μ_q and λ_q are the shear and the bulk viscosity of the phase q, $\boldsymbol{F}_q$ the external body force, $\boldsymbol{F}_{lift,q}$ the lift force, $\boldsymbol{F}_{Vm,q}$ the virtual mass force, $K_{pq} = K_{qp}$ the interphase momentum exchange coefficient, and p the pressure shared by all phases.

The conservation of momentum for S^{th} proppant is expressed by

$$\frac{\partial}{\partial t}(\alpha_s \rho_s \boldsymbol{v}_s) + \nabla \cdot (\alpha_s \rho_s \boldsymbol{v}_s \boldsymbol{v}_s) = -\alpha_s \nabla p - \nabla p_s + \nabla \cdot \overline{\overline{\boldsymbol{\tau}}}_s + \alpha_s \rho_s \boldsymbol{g} + \alpha_s \rho_s (\boldsymbol{F}_s + \boldsymbol{F}_{lift,s} + \boldsymbol{F}_{Vm,s}) + \sum_{l=1}^{n} K_{ls}(\boldsymbol{v}_l - \boldsymbol{v}_s) \tag{6}$$

where p_s is the S^{th} solids pressure [14], and n the total number of phases.

The Gidaspow model [16] is applied for interphase exchange coefficient K_{pq}, which is a combination of the Wen-Yu model [17] and the Ergun equation [18].

The lift force acting on a secondary phase p in a primary phase q is computed from [16]

$$\boldsymbol{F}_{lift} = -0.5 \rho_q \alpha_p \left| \boldsymbol{v}_q - \boldsymbol{v}_p \right| \times (\nabla \times \boldsymbol{v}_q) \tag{7}$$

In case a secondary phase p accelerates relative to the primary phase q, the inertia of the primary-phase exerts a "virtual mass force" on the particles [19]:

$$\boldsymbol{F}_{Vm} = -0.5 \rho_p \alpha_q \left(\frac{\mathrm{d}_q \boldsymbol{v}_q}{\mathrm{d}t} - \frac{\mathrm{d}_p \boldsymbol{v}_p}{\mathrm{d}t} \right) \tag{8}$$

2.3 *Numerical methods*

In the calculation, the governing equations can be written in a generic form:

$$\frac{\partial}{\partial t}(\alpha_k \rho_k \phi_k) + \nabla (\alpha_k \rho_k u_k \phi_k) = \nabla (\alpha_k \Gamma_k \nabla \phi_k) + \alpha_k S_k \tag{9}$$

where the subscript k denotes each phase, ϕ is a physical variable, and Γ_k and S_k the transport coefficient and source term respectively. In the calculation, firstly both the pressure field and the velocity field of the liquid are determined using the SIMPLE algorithm, and then those of the proppant are computed. The volumetric fraction of the proppant particles is calculated with the continuity equation,

and after that, the velocity field is obtained using the momentum equation. Finally, the convergent solutions of fracturing fluid and proppant are determined through iterations.

2.4 *Computation model*

Generally, the geometry of crack after hydraulic fracturing is very complex, and besides, the composition of the fracturing fluid and its movement boundary are different under various conditions. This study is mainly focused on the horizontal migration of proppant under simplified geometry and boundary conditions, that is, the rectangular domain adjacent to the well bore. According to Smith et al.[20], the middle of the left rectangular border and the right border are set as perforating position and the crack section far from the well bore respectively, which are the outlet and the inlet during the fracturing flowback. The remaining borders are all set as solid wall. In Fig.1, the inflow boundary is $x=-5,\ 0<y<1$, and the outflow boundary $x=0,\ 0.4<y<0.7$. Within the computational domain, there is no mass or heat exchange between fracturing fluid ($\rho_f=1\times10^3\,\mathrm{kg/m^3}$, $\nu=0.005\,\mathrm{kg/(m\cdot s)}$) and spherical particles ($\rho_s=2.5\times10^3\,\mathrm{kg/m^3}$, $d=0.001\,\mathrm{m}$).

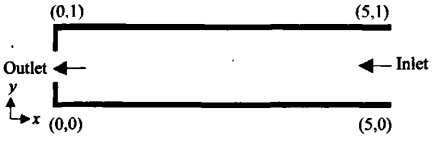

Fig.1 Schematic of physical model

2.5 *Initial and boundary conditions*

In the calculation, the same velocity is set for the fracturing fluid and the proppant at the inlet, and the initial volumetric concentration within the computational domain is equal to that at the inlet. The initial and boundary conditions are:

For fracturing fluid and proppant:

$$V_f=V_s=0$$

The volumetric fraction of proppant:

$$\alpha_s=\alpha_0$$

For inflow boundary:

$$u_f=u_s=U_0,\ v_f=v_s=0,\ \alpha_s=\alpha_0$$

For outflow boundary:

$$\frac{\partial u_f}{\partial x}=\frac{\partial u_s}{\partial x}=0,\ v_f=v_s=0$$

For solid wall:

$$v_f=v_s=0,\ \frac{\partial p}{\partial n}=0$$

3. Results

In Table 1, four cases are considered in the numerical simulation. The flowfields of both the fracturing fluid and the proppant, as well as the distribution of the proppant are determined. The analysis on the proppant's volumetric concentration is also conducted.

Table 1 Simulated cases

	Case 1	Case 2	Case 3	Case 4
U_0	−0.01 m/s	−0.1m/s	−1.0m/s	−0.1m/s
α_0	0.35	0.35	0.35	0.10

3.1 *Qualitative analysis of the flow field*

Case 2 is taken as the example, the flowfield, the fracturing fluid and the proppant are analyzed firstly, and then the flowfield under different conditions are compared.

3.1.1Velocity field

(1) Fracturing fluid

In Fig.2, initially (T=5s) the fracturing fluid mainly flows to the left. The horizontal velocity component in the central region increases gradually (T=30s), and two vortexes are formed. A relatively large combined flow zone appears near the inlet. The velocity is larger in the central part, where fluctuation would occur with the further development of the flowfield (T=80s).

(2) Proppant

In Fig.2, the vertical velocity component of the proppant is downward initially (T=5s) as a result of the gravitational settling. After that (T=30s), the velocity becomes larger in the central part, with a vortex remaining in the lower part. Due to the gravitational sedimentation, no streamline of the proppant exists in the upper part. At T=80s, a rapid-flow zone with fluctuations would appears in the central part.

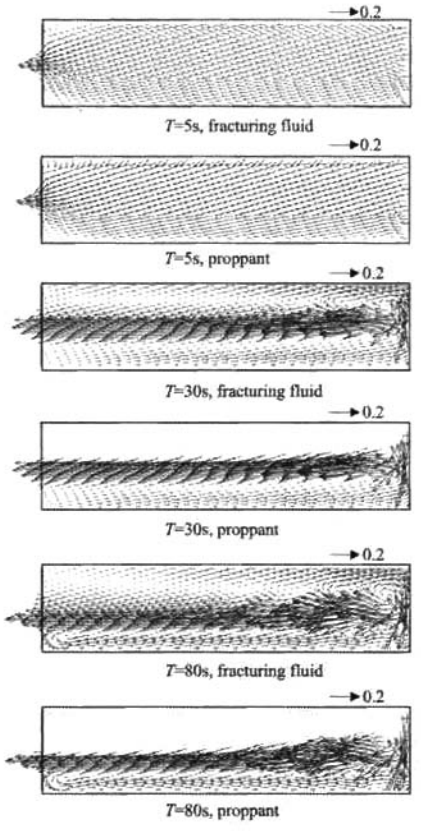

Fig.2 Velocity of the fracturing fluid and proppant in Case 2

3.1.2 Effect of the inlet velocity

(1) Case 1, ($U_0 = -0.01$m/s)

In Fig.3 at T=30s, the flowfield of the fracturing fluid resembles that in Case 2, except that no fluctuation appears in the central part. The proppant also flows in a similar way, with downward velocity component at the interface of the upper blank zone and the rapid-flow one.

(2) Case 3, ($U_0 = -1.0$ m/s)

For T=0s-30s, the flowfields of both the fracturing fluid and the proppant show no obvious difference, indicating that the fracturing fluid exerts almost no effect on the fracturing fluid.

3.1.3 Effect of volumetric concentration

The initial volumetric concentration is 0.10 in Case 4. Consequently the rapid-flow zones of the fracturing fluid and the proppant are smaller compared to Case 2. The proppant velocity is almost zero at the outlet, namely, the proppant accumulative height is smaller than that at the outlet.

3.2 *Variation of proppant volumetric concentration*

It is very effective to control the proppant flowback to enhance the quality of hydraulic fracturing. In the present study, the proppant flowback under different conditions is analyzed through its total volume $\bar{\alpha}$. The fluctuation of the proppant volumetric concentration is expressed by $\bar{\alpha}'$, where $\bar{\alpha}' > 0$ means the inflow exceeds the outflow, and vice versa.

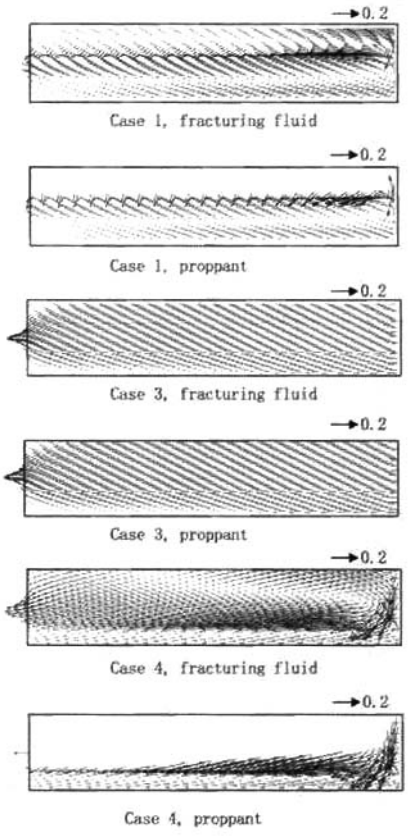

Fig.3 Velocity of fracturing fluid and proppant at T=30s

In Fig.4 the initial averaged volumetric concentration in Cases 1 to 3 is 0.35. In the calculation, the increasing rate of the averaged volumetric concentration is nearly the same despite their difference in the inlet velocity (case 1, $\bar{\alpha}'$ = 0.002/s, case 2, $\bar{\alpha}'$ = 0.0019/s, case 3, $\bar{\alpha}'$ = 0.0021/s). The situation changes as $T > 10$s. For case 1, $\bar{\alpha}'$ = 0.00197/s at an interval of $10\text{s} < T < 40\text{s}$, and gradually declines after reaching the summit at $T = 50$ s, for case 2, $\bar{\alpha}' = 0.00123$s for $10\text{s} < T < 30\text{s}$, and keeps a constant of -0.0024s

when $55\text{s} < T < 70\text{s}$. In case 3, the averaged volumetric concentration almost keeps unchanged from 10 s-50 s. Due to a low initial value of 0.1, the volumetric concentration in case 4 increases rapidly in a range of $0\text{s} < T < 70\text{s}$.

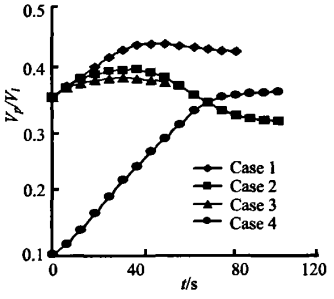

Fig.4 Variation of proppant's volumetric concentration under different conditions

3.3 *Distribution of proppant volumetric concentration*

The evolution of $\bar{\alpha}$ under different conditions is analyzed based on the distribution of α within the computational domain, and the "high-sand-zone" is defined as a zone where the local volumetric concentration is higher than 0.6.

In Fig.5, the inlet velocity is $-0.1\ \text{m/s}$ in Case 2, and the proppant sedimentates rapidly ($4.8\text{m} < x < 5.0\text{m}$) at a distance less than 0.2 m from the inlet. Due to a rapid-flow zone at the interface of the accumulative layer and water, the proppant on the surface is carried downstream. Consequently, the thickness of the high-sand-zone increases gradually within $0\text{m} < x < 4.8\text{m}$ at the initial stage ($T < 36$ s , $\bar{\alpha}$ increases). The high-sand-zone at upstream ($4\text{m} < x < 4.8\text{m}$) accumulates more rapidly than at downstream. As a result, the effective flow section gradually decreases, and finally induces the interface wave and the significant increase of the accumulative thickness downstream (T=60s). With the further development, the high-sand-zone downstream shows no variation in both the shape and the thickness despite remarkable ups and downs of the interface wave upstream.

In Fig.6, the inlet velocity in Case 1 is much less than that in Case 2, and therefore the proppant would sedimentate quickly on the high-sand-zone surface. The proppant would be carried downstream and spread uniformly under the influence of the rapid-flow zone. As the inlet velocity is very low, the averaged velocity at the outlet is merely -0.03 m/s before the high-sand-zone becomes higher than the inlet. The growth rate of α would decrease and finally reach a state of balance.

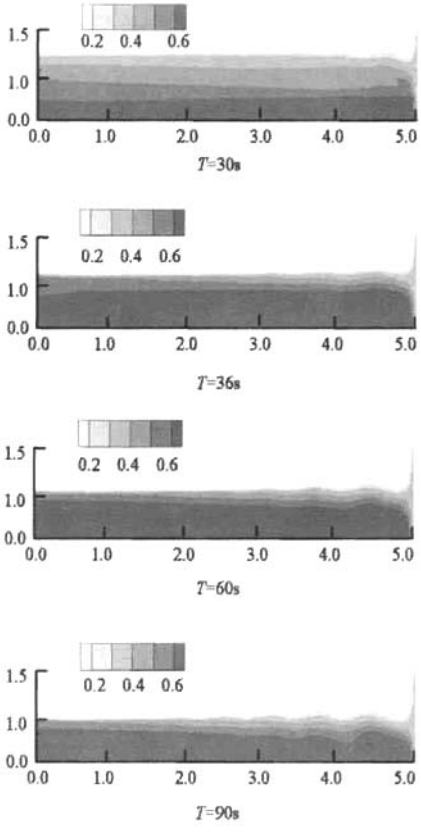

Fig.5 Distribution of α in Case 2

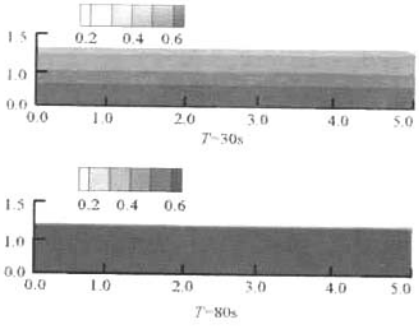

Fig.6 Distribution of α in case 1

In Fig.7, the inlet velocity is relatively large in Case 3, and α shows almost no variation except for two triangle regions near the outlet. As can be seen, vortexex occur in the two triangle regions. In Fig.8. compared to Case 2, the high-sand-zone increases more slowly in Case 4 as a result of lower initial volumetric concentration. The effective flow section is larger, resulting in a lower averaged velocity within quite a long period. The interface is steady except

near the inlet.

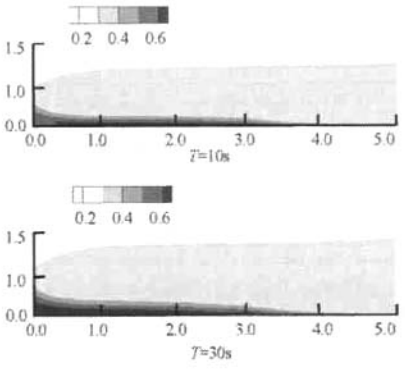

Fig.7 Distribution of α in Case 3

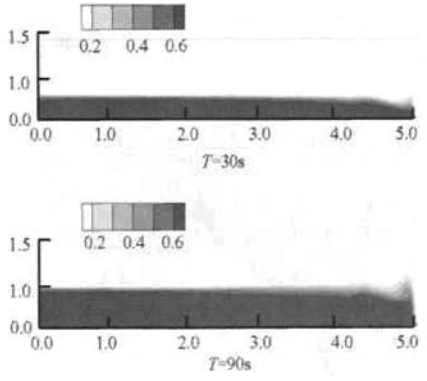

Fig.8 Distribution of α in Case 4

4. Conclusions

The horizontal migration of the proppant at different velocities and volumetric concentrations has been investigated herein with the two-fluid model, and the following conclusions are reached:

(1) Based on the numerical simulation of the proppant horizontal migration at different velocities, the main characteristics of the flowfield and the migration processes are obtained. The results show that three kinds of migrating processes may take place. As the velocity is low (Case 1), the proppant would sedimentate soon after passing the inlet. At the interface of the high-sand-zone and the water, the proppant would be transported rapidly due to the local high stress. The proppant averaged volumetric concentration increases at a relatively high rate before the high-sand-zone is higher than the outlet. At an increased velocity (case 2), the migration processes are similar to those in Case 1 at the initial stage. However, the flow section would gradually decline, resulting in an increase of the actual velocity. The wave-shape dunes are consequently formed due to the instability of the high-sand-zone interface. In case the velocity is higher, the proppant almost exerts no influence on the fracturing fluid.

(2) The simulated results indicate that not only the initial height of the high-sand-zone, but also the increasing rate are relatively low. The velocity is fairly low as a result of large flow section for quite a long period, and thus the high-sand-zone interface is stable, while the proppant averaged volumetric concentration increases at a comparatively high rate.

References

[1] BRINGEDAL B. Ø., MORUD S. A. and HUSEMAN G. *Online water-injection optimization and prevention of* reservoir damage[C]. **SPE 102831.** San Antonio, Texas, USA, 2006, 1-6.

[2] WOLHART S. L., HARTINGM T. A. and YOUNG T. J. Hydraulic fracture diagnostics used to optimize development in the Jonah Field[C]. **SPE 102528.** San Antonio, Texas, USA, 2006, 1-12.

[3] LI Tian-cai, GUO Jian-chun and ZHAO Jin-zhou. Study on the proppant backflow control and the sanding control of fractured gas wells and its application[J]. **Journal of Xi'an Shiyou University (Natural Science),** 2006, 21(3): 44-27 (in Chinese).

[4] CHEN Zhuo, WANG Yi and YANG Qing-yu et al. Research on fracturing optimization for shallow gas reservoirs with low permeability, low temperature, and waters sensitivity[J]. **Natural Gas Industy,** 2006, 26 (8): 99-101 (in Chinese).

[5] LIU Guang-yu, XU Ya-ru. Optimizing fracturing-fluid cleanup in the bossier sand[J]. **Foreign Oil Field Engineering,** 2006, 22(4): 11-15.

[6] YING Xin-ya. Modeling of motion of particle clouds formed by dumping dredged material[J]. **China Ocean Engineering,** 2001, 15(1): 85-96.

[7] MA Fu-xi, LI Zhi-wei. Large eddy simulation of pollutant movement in water[J]. **Journal of Hydraulic Engineering,** 2002, (9): 55-59(in Chinese).

[8] LIU Yong-bing, CHEN Ji-zhong and YANG Yong-rong. Numerical simulation of liquid-solid two-phase flow in slurry pipeline transportation[J]. **Journal of Zhejiang University (Engineering Science),** 2006, 40(5): 858-863(in Chinese).

[9] ANDERSON T. B., JACKSON R. A fluid mechanical description of fluidized beds[J]. **I and EC Fundam.,** 1967, 6: 527-534.

[10] HUANG Sui-liang, JIA Y. F. and WANG Sam S. Y. Numerical modeling of suspended sediment transport in channel bends [J]. **Jounral of Hydrodynamics, Ser. B,** 2006, 18 (4): 411 - 417.

[11] ZHOU Yong, WU Ying-xiang and ZHENG Zhi-chu et al. Research on oil-water separation technique I – numerical simulation in both straight and helical pipes[J].

Journal of Hydrodynamics, Ser. A, 2004, 19 (4): 540-546 (in Chinese).

[12] ALDER B. J., WAINWRIGHT T. E. Studies in molecular dynamics II: behaviour of a small number of elastic spheres[J]. **J. Chem. Phys.** , 1960, 33: 1439-1451.

[13] ERINGEN A. C. **Continuum physics**[M]. New York, USA: Academic Press, 1976, 1-127.

[14] MA D., AHMADI G. A thermodynamical formulation for dispersed multiphase turbulent flows[J]. **Int. J. Multiphase Flow,** 1990, 16: 323-351.

[15] WANG Jia-jun, GU Xue-ping and YANG Fu-jun et al. Effects of restitution coefficient and drag force on gas-solid flow behavior: a two-fluid model simulation[J]. **Jouranal of Chemical Engineering of Chinese Universities,** 2006, 20(2): 164-168(in Chinese).

[16] GIDASPOW D., BEZBURUAH R. and DING J. Hydrodynamics of circulating fluidized beds[C]. **Proceeding of the 7th Engineering Foundation Conference on Fluidization.** Brisbane, Australia, 1992, 75-82.

[17] WEN C. Y., YU Y. H. Mechanics of fluidization[J]. **Chemical Engineering Progress,** 1966, 62(4): 100-111.

[18] ERGUN S. Fluid Flow through packed columns[J]. **Chemical Engineering Progress,** 1952, 48(2): 89-94.

[19] DREW D. A., LAHEY R. T. **In particulate two-phase flown**[M]. Boston, USA: Butterworth- Heinemann, 1993, 509-566.

[20] SMITH M. B., BALE A. L. and BRIT K. T. et al. Enhanced 2D proppant transport simulation: the key to understanding proppant flowback and post-frac productivity[C]. **SPE 38610.** San Antonio, Texas, USA, 1997, 1-8.